Available online at www.sciencedirect.com

SciVerse ScienceDirect

Journal of the European Ceramic Society 32 (2012) 2253–2265

www.elsevier.com/locate/jeurceramsoc

Interfacial behavior on Al_2O_3/HAYNES® 214™ joints fabricated by solid state bonding technique with Ni or Cu–Ni–Cu interlayers

M.L. Hattali [a,b,*], S. Valette [a], F. Ropital [b], N. Mesrati [c], D. Tréheux [a]

[a] *Laboratoire de Tribologie et Dynamique des Systèmes, UMR CNRS ECL ENISE ENSMSE 5513, École Centrale de Lyon, 69134 Ecully Cedex, France*
[b] *IFP Energies nouvelles, Rond-point de l'échangeur de Solaize, BP 3, 69360 Solaize, France*
[c] *Laboratoire de Sciences et Génie des Matériaux, École Nationale Polytechnique d'Alger, 10, avenue de Hassen Badi, EL harrach Alger, Algeria*

Received 11 April 2011; received in revised form 23 January 2012; accepted 26 January 2012
Available online 8 March 2012

Abstract

The residual stresses due to the difference in thermal expansion between ceramic and metal is a significant parameter to control during the fabrication of ceramics/metal joint. In this work, residual stress distribution, after solid state bonding of different joints, was measured using X-ray diffraction (XRD) and Vickers Indentation Fracture (VIF) methods. Tensile stress concentration in alumina caused by the thermal expansion mismatch in the Al_2O_3/Ni/Ni alloy (HAYNES® 214™) joint severely deteriorated the assembly and caused cracks in alumina. To solve this problem, this paper shows that the use of a Cu/Ni/Cu multi-layer, associated with the direct copper bonding method (DCB), by pre-oxidation of copper, reduces significantly the tensile residual stresses in alumina material. Consequently, this process offers the possibility of producing an interlayer with a high melting temperature and hence joints which can withstand high-temperatures.

Keywords: Joining; Interface; Toughness; Residual stress; Al_2O_3

1. Introduction

The realization of metal–ceramic joints is often unavoidable, both for research of contradictory use properties and resolution of technological difficulties.[1–12] The performance of the bonded material is often influenced and controlled by the ceramic–metal interface properties (mechanical, electrical, magnetic and chemical).[9–12] Till now, several techniques for joining ceramics to metals have been developed.[13–23] Every technology has its advantages and disadvantages.[22]

In this study, we have used the classic solid state bonding process,[1,4,11,22] with insertion of an metal interlayer, associated or not with the direct copper bonding technique (DCB).[21] The interlayer can reduce cracking, relax the thermal residual stress and improve the joining strength. However, making a metal–ceramic joint involves inevitably residual stresses when the bonded assembly cools from the joining temperature to room temperature. These stresses influence the strength and fracture energy of the bond.[23,24] The stress field depends on many factors, e.g. elastic and plastic properties of materials to be joined as a function of temperature, thermal expansion coefficients, geometric design[4,25] of the assembly. Numerous works are available to measure residual stresses by neutron[1,26,27] or X-ray diffractions (XRD)[28,29] or other less precise methods including Vickers Indentation Fracture (VIF) method[1,28] and removal layer techniques.[28] In parallel, a variety of analytical and numerical models were developed to understand and optimize the residual stress state in metal–ceramics joints.[30,31] But rarely were they compared to experimental measurements, with results of classical XRD and indentation fracture methods. The most complete comparison was made by Guipont.[28]

Recently,[1] we calculated (FEM) and measured (XRD, VIF) the residual stress distribution in alumina/Ni/alumina and alumina/Ni/nickel alloy systems.[1] The principal conclusions can be summarized as follows:

- The results of the three employed methods (FEM, XRD and VIF) show that the highest tensile stress is concentrated at the boundary of the outer surface of the joint, and it will

* Corresponding author. Present address: CEA, IRAMIS, SPCSI, Group Complex Systems and Fracture, 91191 Gif sur Yvette, France. Tel.: +33 472186517; fax: +33 478331140.
E-mail address: hattali.lamine@gmail.com (M.L. Hattali).

0955-2219/$ – see front matter © 2012 Elsevier Ltd. All rights reserved.
doi:10.1016/j.jeurceramsoc.2012.01.036

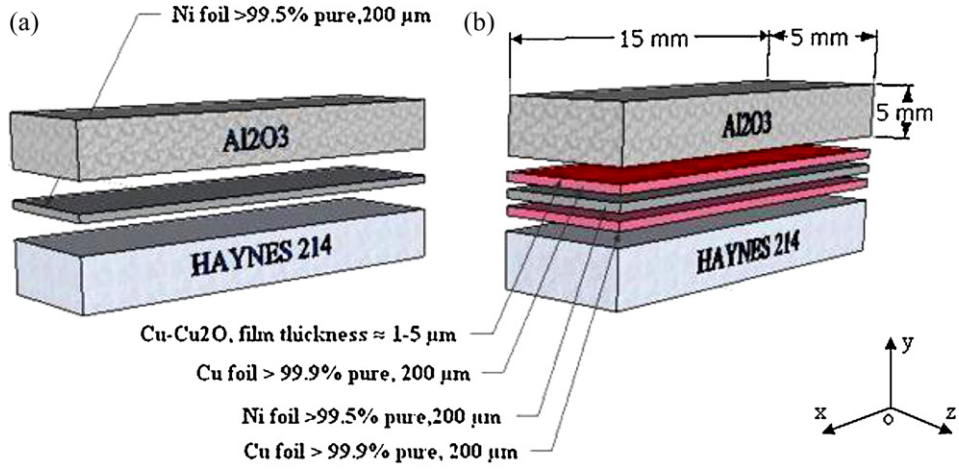

Fig. 1. Schematic illustration of a Al_2O_3/HAYNES® 214™ joint (a) with Ni interlayer and (b) with Cu_2O–Cu/Ni/Cu interlayer.

cause cracks in alumina layer only in the case of dissimilar Al_2O_3/Ni/HAYNES® 214™ bonds, because the maximum residual tensile stress of Al_2O_3/Ni/Al_2O_3 specimen was lower than that of the Al_2O_3/Ni/HAYNES® 214™ specimen.

- FEM and X-ray results are in rather good agreement, knowing that certain phenomena, such as grain boundary diffusion of nickel in alumina, are not taken into account. The indentation method seems to over-estimate the stresses, but takes into account the fall of ceramics properties (in particular their toughness) close to the interface, which is not taken into account in FEM and XRD.

To minimize the stresses in the Al_2O_3/Ni/HAYNES® 214™ system, we propose to replace the nickel foil by a Ni–Cu–Ni multi-layer. Moreover the choice of copper will allow us to use DCB (or gas–metal eutectic) method[21,32–35] and, in consequence, of working in brazing condition, i.e. with a weak applied pressure during the bonding.

DCB method is based on a binary eutectic system[36] to join alloys and ceramics. An interlayer is required to form a liquid eutectic phase and wet ceramics at high temperature. The joint is formed through inter-diffusion between interlayer and parent materials. The relation between wetting behavior and bonding adhesion in Al_2O_3/Cu interfaces has attracted interest in the literature.[37,38] Between 1065 °C and 1085 °C, copper reacts with oxygen on the surface of the ceramic to form a liquid eutectic [Cu–O]. The liquid phase wets ceramics, eliminates the holes at interface and accelerates the bonding. The excellent wetting of Al_2O_3 by the [Cu–O] liquid followed by the growth of reaction product ($CuAl_2O_4$, or $CuAlO_2$), respectively due to the reaction between CuO and Cu_2O and Al_2O_3, explains the good strength of DCB bonds.[39–41] Compared with solid state bonding, during DCB, the movement of atoms in liquid is quicker, so joining time and pressures are reduced.

The residual stress distribution was measured by X-ray diffraction and indentation fracture methods (VIF) and compared for both systems containing Ni and Cu/Ni/Cu interlayer. In parallel, the interfacial fracture energy and the metal–ceramics fracture strength are determined in order to confirm the role of the residual stresses on the mechanical strength of the assemblies.

2. Experimental procedure

2.1. Materials

As in the previous study,[1] the ceramic material used in this work is a commercial polycrystalline α-Al_2O_3 (AL23 alumina), from UMICORE Marketing services. The alloy is the nickel super alloy HAYNES® 214™ (75% Ni, 16% Cr, 4.5% Al, 3% Fe), which is widely used in technological applications at high temperatures and in severe chemical atmosphere such as that encountered in industrial heating market (petrochemical, etc.). Both base material blocks were machined into small pieces with the dimension of $15 \times 5 \times 5\,mm^3$ (Fig. 1). The metal foils used as filler materials were commercially available and the pure metals or the foils were of high purity. Both Ni and Cu foils were prepared by cold rolling down to a thickness of 200 µm and 100 µm, respectively and had the same dimensions of material blocks. In order to show the influence of the ceramic/metal thickness ratio on the fracture energy, other specific samples were used for "delamination" bending tests (Fig. 2b). Table 1 shows the main characteristics of the metal foils.

To favor "mechanical adhesion", prior bonding, the faying surfaces of HAYNES® 214™ and alumina were machined to obtain surface roughness equal to 0.08 and 0.48 µm, respectively. After machining, all base materials were ultrasonically cleaned in acetone for 30 min, and then blown dry with a heat gun. Cleaned alumina substrate were placed in a high-purity alumina crucible, covered, and then annealed in air at 950 °C for 5 h to completely remove residual organic surface contaminants.

2.2. Bonding processes

After drying in hot air, the base material blocks and the interlayer foils were prepared as block/foil/block sandwiched assembly (Fig. 1). Bonding was achieved in vacuum (10^{-3} Pa).

Table 1
Characteristics and properties of the metal foils.

Metal	Purity (%)	Melting point	Linear exp.coeff. at 0–100 °C (K^{-1})[a]	Young's modulus (GPa)
Ni	99.5	1453	13.1×10^{-6}	205
Cu	99.9	1083	17.0×10^{-6}	129.8

[a] Linear expansion coefficient of alumina and HAYNES® 214™ are 8.1×10^{-6} and 13.3×10^{-6}, respectively.

For Al_2O_3/Ni/HAYNES® 214™ system the temperature was ramped to 1150 °C at 200 °C/h, maintained at 1150 °C for 1 h, and then ramped down to room temperature at 150 °C/h (Fig. 1). During this cycle, a pressure of 16 MPa was applied through a pneumatic piston during the entire cycle.[25] The experimental conditions were selected taking into account previous studies for the systems Al_2O_3/Ni/Al_2O_3 and Al_2O_3/Ni/HAYNES® 214™.[1,4,25,42,43]

These conditions correspond to an optimization of the mechanical properties of the assembly taking into account the parameters of solid-state-bonding (temperature, pressure and time, geometries of the interlayer (ratio thickness/width) and of the system ceramic/alloy, residual stresses, etc.).[1,4]

For Al_2O_3/Cu–Ni–Cu/HAYNES® 214™ system, the process was as follows: firstly, copper foils (100 μm thick) are polished with a 6 μm diamond paste, and oxidized under low oxygen pressure (10^{-3} Pa) at 950 °C for 0.5 h to obtain a superficial adherent Cu_2O film.[41,43] Cu_2O is removed from one of the copper faces in contact with nickel. Thus obtained Cu_2O–Cu/Ni/Cu multilayer, was placed between the alumina and HAYNES® 214™ substrates, checked for good metal–ceramic contact (Fig. 1). Secondly, the parts were heated in a tube furnace in the temperature of 1075 °C at 200 °C/h, maintained at 1075 °C for 10 min, and then ramped down to room temperature at 150 °C/h. During this cycle, the vacuum in the furnace was maintained at 10^{-3} Pa. A minimum low pressure of 1 MPa was applied on the assembly during the entire cycle. In the temperature range of 1065–1083 °C a liquid eutectic phase appears at the Cu_2O–Cu interface; its amount can be controlled by careful regulation of oxide growth on the copper foil. This thin molten film produces an intimate contact between copper and alumina and generates, after cooling, a strong bond between the two materials.

The different bonding conditions are summarized in Table 2.

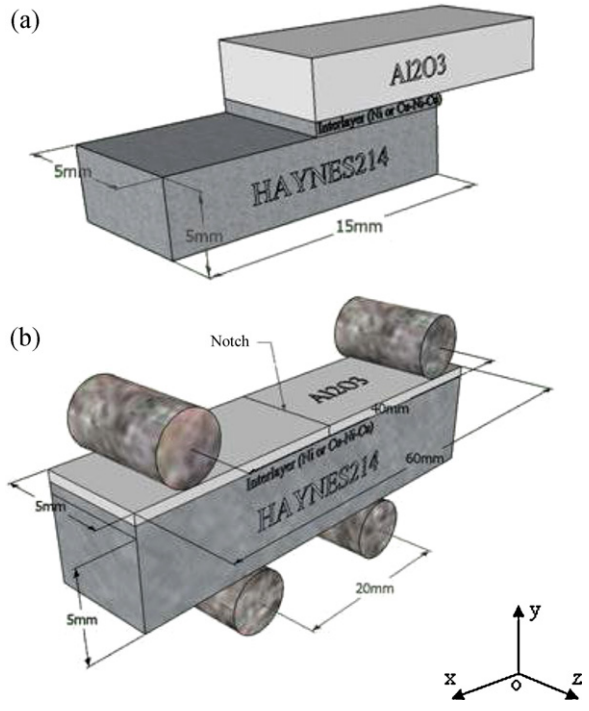

Fig. 2. Schematic of the mechanical test and geometry adapted to the test: (a) mechanical shear test and (b) Four-point 'delamination' bending test.

2.3. Characterization techniques

2.3.1. SEM/EDS

After bonding, the interfacial regions and the fracture surfaces of ceramic/metal joints were observed and analyzed by Scanning Electron Microscopy (SEM) and Energy Dispersive Spectroscopy (EDS), in order to evaluate the morphology and microchemistry of the interfaces and diffusion phenomena. Line scans were conducted perpendicular to the interface. The beam size is typically on the order of 1 μm, and a typical detection limit is ≤1 at.%, and thus, we anticipated that this method might provide information on the extent of homogenization achieved during the bonding cycle.

2.3.2. Mechanical tests

The fracture strength of the joint at room temperature was evaluated using shear test (Fig. 2a). In order to ensure greater accuracy three samples were tested for each joining condition. Shear strength measurements were performed using an Adamel DY25 testing machine (Fig. 2a). The testing was carried out at the constant crosshead speed of 0.1 mm/min, and the strength was calculated by the load at break divided by the nominal area of the joint. Even if a pure shear stress field does not necessarily occur in this testing technique, it is, nonetheless, a suitable means for comparative evaluations. The fracture energy of the assembly is measured using a four-point "delamination" bending test.[44] The sample was mounted on a device which was set up on an Adamel DY25 tensile-compression machine. Sample dimensions were 60×5 mm^2 (Fig. 2b). A thin notch was machined in the median cross section of all the ceramic thickness to serve as crack initiation (Fig. 2b). In order to follow the initiation and the propagation of the interfacial crack, a polished longitudinal side plane of the sample was observed during the test using a magnifying glass. The inner and outer spans were 20 and 40 mm, respectively and the loading rate was 0.1 mm/min. The phase angle for this geometry was ∼44°. Interface cracks in the as-bonded specimens were propagated in steady-state regime. According

Table 2
Experimental conditions for the joining of alumina with HAYNES® 214™ for different metallic foils (Ni and Cu_2O–Cu/Ni/Cu).

System	Temperature (°C)	Time (h)	$e_{interlayer}$ (μm)	Pressure (MPa)	Vacuum (Pa)
Al_2O_3/Ni/HAYNES® 214™	1150	1	200	16	10^{-3}
Al_2O_3/Cu/Ni/Cu/HAYNES® 214™	1075	0.5	100–200–100	1	10^{-3}

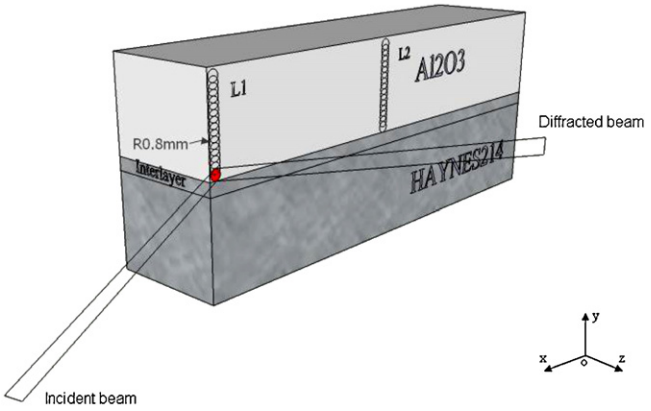

Fig. 3. Schematic representation of the specimen for XRD measurements.

to this geometry, fracture energy can be measured directly by the estimation of the energy dissipated rate G_{IC}, which is calculated using Euler–Bernouilli theory[44,45] as following:

With:

$$G_{IC} = \frac{3}{2}\frac{P^2 l^2 (1-\nu_2^2)}{E_2 h^3 b^2}\left(\frac{1}{(h_2/h)^3} - \frac{\lambda}{((h_1/h)^3 + \lambda(h_2/h)^3 + 3\lambda(h_1h_2/h^2)((h_1/h)+\lambda(h_2/h)^{-1}))}\right) \quad (1)$$

$$\lambda = E_2\frac{(1-\nu_1^2)}{(E_1(1-\nu_2^2))} \quad (2)$$

where P is the first fracture or delamination strength; E_2 is the Ni alloy Young's modulus; E_1 is the ceramic Young's modulus; ν_2 is the Ni alloy Poisson's ratio; ν_1 is the ceramic Poisson's ratio; h_2 is the Ni alloy thickness; h_1 is the ceramic thickness; $h = h_2 + h_1$; b is the sample width; l is the distance between internal and external alumina blocks.

2.3.3. X-ray diffraction method (XRD)

In order to estimate the magnitude and distribution of the residual stresses in the joints, X-ray diffraction method was used. Residual stress measurements were carried out using the $\sin^2\Psi$ method with Ψ goniometer (Dosophatex) and INEL software equipments, at 30 kV, 30 mA.[1] The size of the collimated X-ray beam ($CrK_{\alpha 1}$) for residual stress measurement was ∅800 μm. Measurements were performed with the (3 0 0) peak of alumina at $2\Theta = 113°$. The experimental conditions are identical to those previously used.[1] The different specimens were scanned along two different directions (L1 and L2 in Fig. 3) perpendicular to the metal–ceramics interface. L1-line was at the free end of the specimen, and L2-line was located in the centre of the specimen (Fig. 3). This choice was made taking into account the mapping of complex stress fields calculated previously by FEA[1] for the system Al_2O_3/Ni/HAYNES® 214™. L1 is an area of particularly high tensile stresses, while L2 is an area of softer stresses. The peak positions were determined with commercial software using a pseudo Voight function to fit the data. The peak position was plotted as a function of $\sin^2\Psi$ to evidence shear stresses and data scatter. Finally, the strain and stresses were calculated.

2.3.4. Vickers Indentation Fracture (VIF) method

The indentation method is a standard method for the determination of the critical stress intensity factor K_{IC} (see, e.g. Refs.1,46 for advantage and disadvantage of VIF method). This method was adopted because it can be used on small samples and small size of the analysis area (local analysis). For our study, this method will therefore measure very close to the interface. The residual stress of the joints was also evaluated by indentation method. Based on the calculation of the difference between the lengths of cracks observed induced by indentations for the same ceramic before and after joining.[46] A Vickers indenter was impressed at several points in the ceramics at different distances from the interface on the edge of the joint (line 1 – Fig. 3). In the present investigation, the tests were conducted at a load of 300 g with a loading duration of 15 s every 50 μm, in staggered, from the metal–ceramic interface to ceramic bulk. A Vickers indent may produce two types of cracks, i.e. a system of median cracks and system of Plamqvist cracks. Liang et al.[46] have proposed a unified formula which enables the determination of toughness (K_{IC}) in both cases of median and Palmqvist's fracture modes. The formula is claimed for the use of any load during indentation test:

$$K_{IC} = \frac{H_v a^{1/2}}{\alpha}\left(\frac{E\varphi}{H_v}\right)^{0.4}\left(\frac{C}{a}\right)^{(C/18a)-1.51} \quad (3)$$

Where

$$\alpha = 14\left[1 - 8\left(\frac{4\nu - 0.5}{1-\nu}\right)^4\right] \quad (4)$$

where a and $2C$ are respectively the half-diagonal length of the indent and the average length of radial cracks produced by indentation (see Fig. 4), φ is a constant stress factor ~ 3, ν is Poisson's ratio, H_v is the hardness and E is the Young's modulus of the material.

In addition, the residual stress in ceramics can be calculated by using the following equation[47]:

$$\sigma_s = \frac{K_{IC}}{(\pi C\Omega)^{1/2}}\left[1 - \left(\frac{C_0}{C}\right)^{3/2}\right] \quad (5)$$

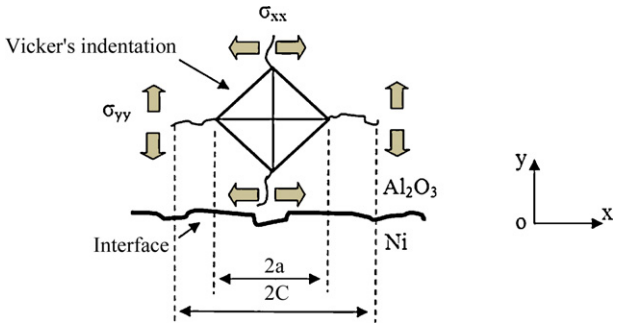

Fig. 4. Indentation fracture method, where $2a$ is the indent diagonal and $2C$ is the total length of the radial crack. For residual stress calculation (σ_{yy}) we take into account only the crack length parallel to the interface.

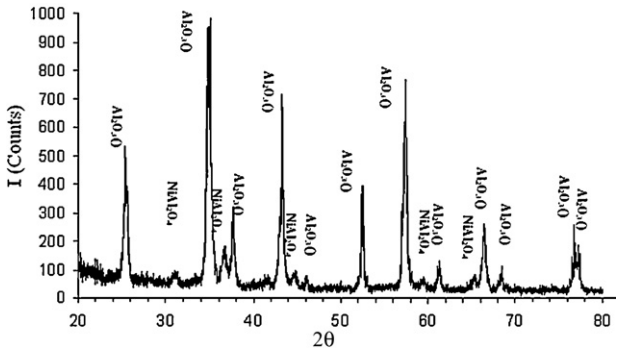

Fig. 6. GIXRD patterns of high purity alumina bonding area collected at an incidence angle of 5° ($k_{K\alpha}$ Cu).

where K_{IC} is the substrate toughness, $2C_0$ is the average length of radial cracks before joining, $2C$ is the average length of radial cracks parallel to metal–ceramics interface and Ω is a constant depending on crack geometry ($\Omega = 4/\pi^2$). In this case where $C < C_0$, σ_s is negative and the stresses are compressive.

3. Results and discussion

3.1. Interfacial microstructure

3.1.1. Al_2O_3/Ni/Haynes® 214™ system

The microstructure and microchemistry of polished cross-section of Al_2O_3/Ni/HAYNES® 214™ joint are shown in Fig. 5. The Ni foil adheres to the ceramic and fills up the pores in the surface. The presence of Ni inside the alumina pores was detected up to a depth of about 10 μm from the interface. The uniaxial applied pressure (16 MPa) was responsible for slight decrease in metal layer thickness. Reaction between Ni and Al_2O_3 strongly depends on temperature, time and atmosphere. Under the adopted experimental conditions chemical reactions are likely to occur between the Ni and Al_2O_3. The cross section of the Al_2O_3/Ni interface formed by diffusion bonding at 1150 °C for 1 h, using a 0.2 mm interlayer, is characterized by EDS microanalysis and Grazing incidence X-ray diffraction (GIXRD). The GIXRD patterns collected at an incidence angle of 5° are shown in Fig. 6. The spinel $NiAl_2O_4$ has been found as an interface suggests the oxygen activity in the system is relatively high. Numerous studies have analyzed the Al_2O_3–Ni system both experimentally and thermodynamically. The spinel $NiAl_2O_4$ has often been found as an interphase. The reaction mechanism generally suggested for its formation involves a NiO intermediate[48]:

$$Al_2O_3 + NiO \Rightarrow NiAl_2O_4 \quad (6)$$

With an associated free energy change of $\Delta G = -6000 - 9.5\,T$ (J mol^{-1}).[48]

From thermodynamic point of view the oxidation of Ni is related to the low level of vacuum (10^{-3} Pa) inside the furnace or to the oxygen dissolved in Ni.

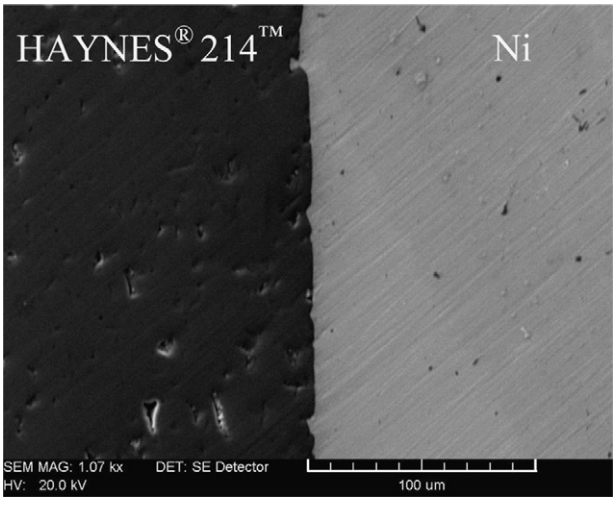

Fig. 5. Sample Al_2O_3/Ni/HAYNES® 214™ (1150 °C for 1 h; 16 MPa pressure): SEM image of polished cross-section perpendicular to the Ni–Al_2O_3 interface.

3.1.2. Al_2O_3/Cu_2O–Cu–Ni–Cu/HAYNES® 214™ system

Multiple microprobe scans were performed on the samples, and information on the aluminum, oxygen, copper and nickel concentrations were obtained. The scan indicates three regions: (1) alumina, (2) the interlayer, and (3) Ni-based super-alloy (HAYNES™ 214®) (Figs. 7 and 8). In the alumina, the Al/O ratio is as expected for Al_2O_3. The presence of Cu inside the alumina pores was detected up to a depth of about 10 μm from the interface. Within the interlayer, the aluminium and oxygen contents are very low or below detection limits. Within a region, 5–10 μm thick. The Cu in the Cu–Ni interface is about 40 at.% and decrease as the centre of the interlayer. The conditions used for pre-oxidation of copper, identical to our previous studies,[41,43] lead to the growth of Cu_2O in accordance with the thermodynamic data[49] indicating that oxidation of copper to Cu_2O at 1000 °C is expected when the copper activity exceeds 4%. Quantitative analysis by EDX has revealed the growth, in the copper zone, of a spheroidal phase identified as Cu_2O (Fig. 8). The formation of the Cu–O liquid eutectic is thus confirmed, because the eutectic is transformed in a two-phase zone Cu–Cu_2O after solidification.

The pre-oxidized copper thickness, near alumina is reduced after bonding (~70 μm thick; initial thickness about 100 μm) because part of the interlayer fills very well the porosity and

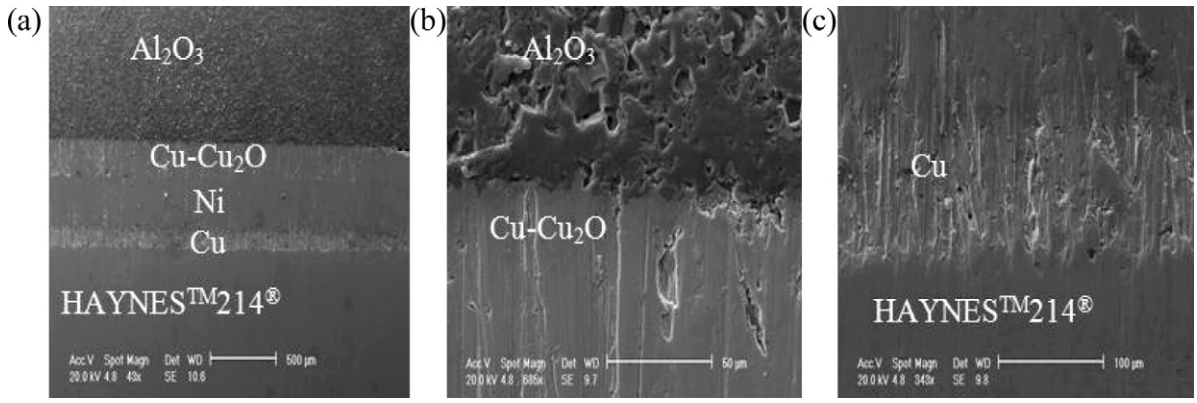

Fig. 7. Sample Al_2O_3/Cu_2O–Cu/Ni/Cu/HAYNES® 214™ (1075 °C for 0.5 h; 1 MPa pressure): (a) SEM image of polished cross-section perpendicular to the interfaces, (b) Al_2O_3/Cu–Cu_2O interface, and (c) Cu/HAYNES® 214™ interface.

roughness of the ceramic due to fusion of the "copper–oxygen eutectic".[50] This thinning, due to partial fusion, is more significant than that observed for copper interlayer near the HAYNES™ 214® (~90 μm thick – initial thickness about 100 μm), only due to copper creep. While in the nickel, the decrease from 200 μm to about 180 μm is also related to creep effect.

Because we have worked in the same experimental conditions as Courbiere[41] and Kara-Slimane[43] we suppose that $CuAlO_2$ is likely present in the Cu–Cu_2O/Al_2O_3 interface. Also, the presence of $CuAlO_2$ induces higher bond strengths[43,50] than those of interfaces that do not contain $CuAlO_2$. The good adhesion, obtained in this sample, can be correlated not only with the good wet-ability of Cu–O liquid eutectic, present at the beginning of brazing (DCB)[41,43] but also with the deformability of $CuAlO_2$.[41]

3.2. Residual stresses

The residual stress (σ_{yy}), along which the interface of the joint peels or cracks, is mainly discussed because this stress (σ_{yy}) is considered to influence the strength of the joint. Tension stress concentration near the specimen edge can cause fracture within the ceramics, in the case of strongly bonded systems, or delamination at the interface, for weakly bonded systems. σ_{yy} governs the fracture mode I of energy release rate. The second significant stress is the shear stress (σ_{xy}). This latter, in combination with the tensile stresses that are present, can induce fracturing along the ceramic–metal interface. It governs the mode II of energy release rate.

3.2.1. X-ray stress measurements

As an example Fig. 9a shows the feature of the various peaks of alumina recorded for $\Psi = -50°$ to $+50°$ and Fig. 9b and c are examples of $\varepsilon_{\varphi\psi} = f(\sin^2\psi)$, in alumina after assembly. It will be noted that far from Al_2O_3/Ni interface ($1\,mm \leq d \leq 4\,mm$), the elliptic form is well observed, sign of a homogeneous and isotropic material, which validates values of stresses deduced from measurements (Fig. 9b). Contrariwise, close to the Al_2O_3/Ni interface ($0.5\,mm \leq d < 1\,mm$) (Fig. 9c), we observe no regular form of $\varepsilon_{\varphi\psi} = f(\sin^2\psi)$ that synonym of local anysotropic residual stress (residual stress gradient) and, as a result, of flawed measures.

X-ray stress is estimated on the alumina side along two lines perpendicular to the interface, located at two different distances from the free surface: one passing through the center of the sample (L2) and the other near the edge (L1) (see Fig. 3).

Both the shear stress (σ_{xy}) (Fig. 10) and the axial (perpendicular) stress (σ_{yy}) (Fig. 11) data are shown, along with errors

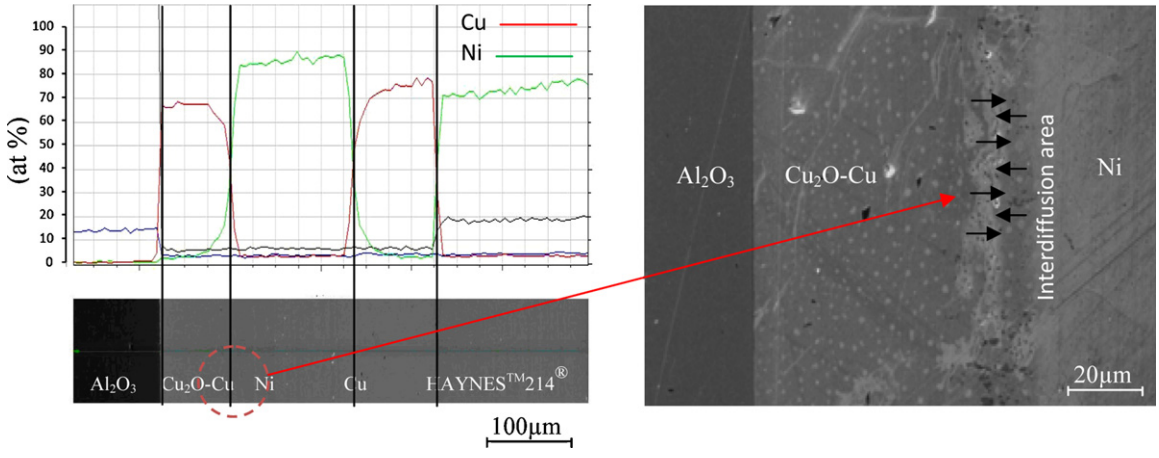

Fig. 8. Chemical profile in the interlayer of an as-bonded simple as determined by EDS. Substantial penetration of copper into nickel is indicated.

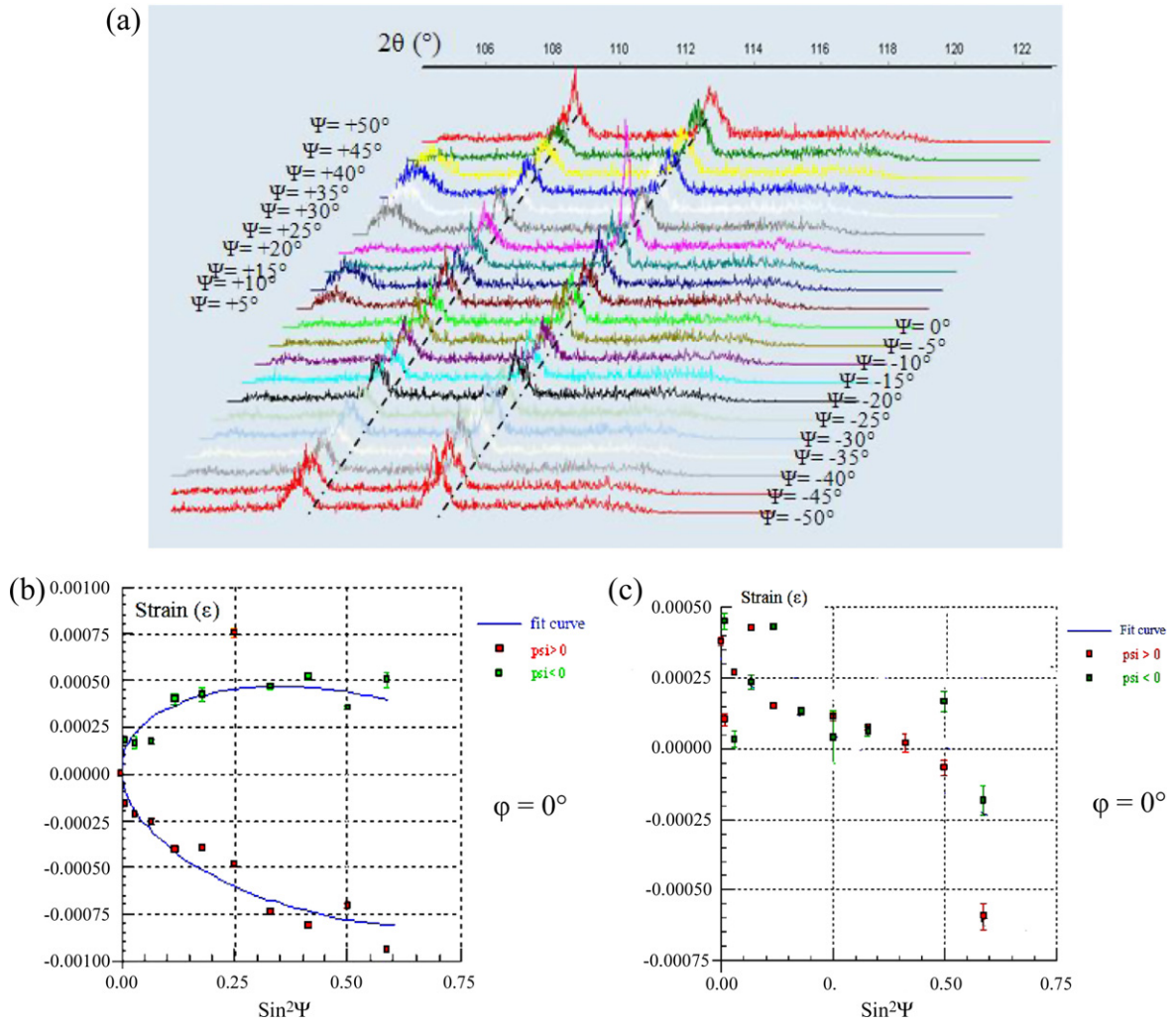

Fig. 9. (a) $\theta - 2\theta$ XRD pattern of Al_2O_3 (3 0 0) at diferentes ψ angles for Al_2O_3/Ni/HAYNES® 214™ joint. Example of $\varepsilon_{\varphi\psi} = f(\sin^2\psi)$ plots and (b) far to the interface (1 mm $\leq d \leq$ 4 mm), no residual stress gradient observed. (c) Near to the interface (0.5 mm $\leq d <$ 1 mm), residual stress gradients were observed.

estimated from standard deviations of the least squares fitting of the recorded diffraction profiles. For the two studied systems the shape of the curves is qualitatively similar except in the case of the shear stress σ_{xy} at the vicinity of the interface (L1) (Fig. 10a). This later (shear stress σ_{xy}) is in tensile stress in the case of Ni interlayer and in compressive stress in the case of Cu interlayer. These compressive stresses show that the use of Cu–Ni multilayer is favorable. However, at the center (L2), the shear stresses (σ_{xy}) appeared to be close to zero or compressive (Fig. 10b).

The axial stress (σ_{yy}) appeared to be compressive stress at the center (L2) (Fig. 11b), near the interface, and become negligible in the ceramic bulk. It was favorable to the metal–ceramic bond, and it could be regarded as one part of the bond strength of metal–ceramic. At the edge of the assembly (L1), strong tensile stresses were measured. Their magnitude roughly decreases with the distance to the interface and becomes almost constantly zero (Figs. 11a and b). It will however be noted the beneficial effect of the multilayer Cu–Ni–Cu since the residual stresses in the Al_2O_3/Ni/HAYNES® 214™ system, at 0.5 mm from interface is 201 ± 53 MPa, whereas for Al_2O_3/Cu–Ni–Cu/HAYNES® 214™ system the stresses are reduced to 107 ± 32 MPa, i.e. close to those measured for the Al_2O_3/Ni/Al_2O_3 system (108 ± 53).[1] This result indicates a higher probability of failure produced by a thermo-mechanical loading. Note that these stress measurements are qualitatively in agreement with the finite element (FEA) calculations which are detailed in our previous paper.[1] We note in particular that the free edge of the sample (corresponding to L1) is particularly stressed, in tension.

3.2.2. *Vickers Indentation Fracture method*

Vickers indentations (applied load 3 N) were performed in alumina from the metal ceramic interface to the ceramic bulk for both Al_2O_3/Ni/HAYNES® 214™ and Al_2O_3/Cu–Ni–Cu/HAYNES® 214™ joints. The variation of apparent-toughness of alumina after bonding versus distance from interface was identified near the free edge (L1). Seeing that the stress values are lower along L2, we limited the VIF analysis in the more critical direction L1. Fig. 12a shows a decrease in the ceramic apparent-toughness near the interface. For Al_2O_3/Ni/HAYNES® 214™ joints, the alumina toughness drops from 5.8 ± 0.4 MPa $m^{1/2}$ before bonding, to about

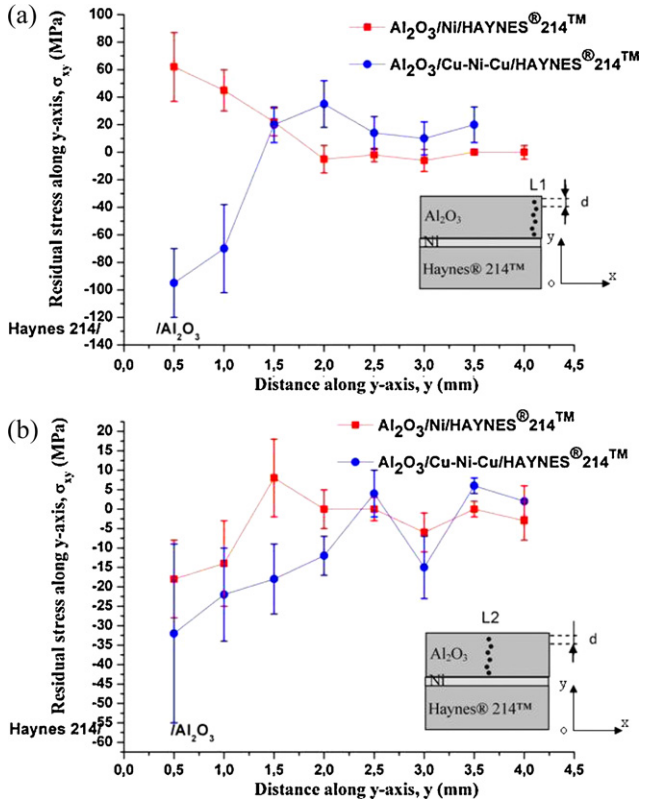

Fig. 10. The residual shear stress (σ_{xy}) distribution (XRD measurements) on the alumina ceramic close to the interface for both Al_2O_3/Ni/HAYNES® 214™ and Al_2O_3/Cu_2O–Cu/Ni/Cu/HAYNES® 214™ joints ($d = 0.5$ mm). (a) L1 and (b) L2.

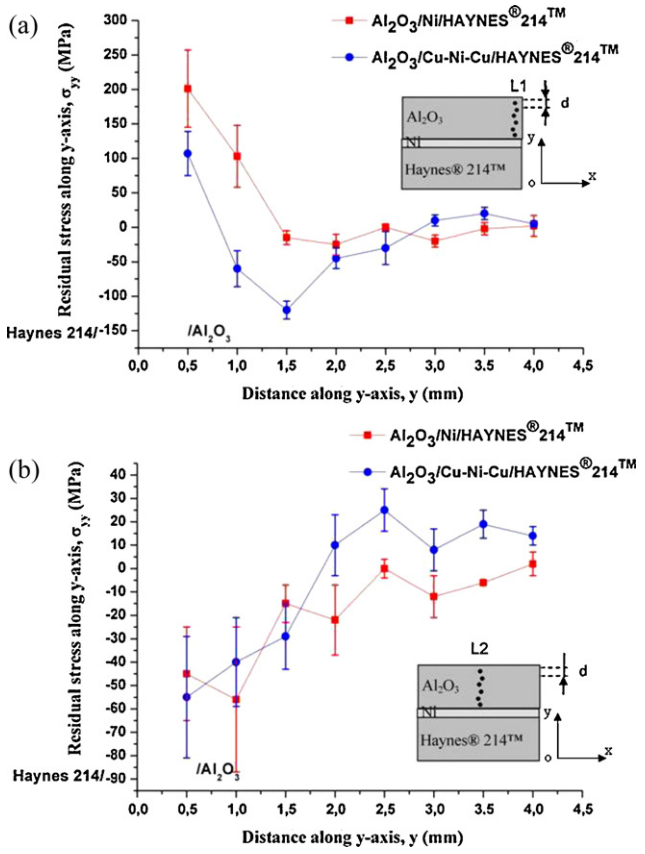

Fig. 11. The residual stress (σ_{yy}) distribution (XRD measurements) on the alumina ceramic close to the interface for both Al_2O_3/Ni/HAYNES® 214™ and Al_2O_3/Cu_2O–Cu/Ni/Cu/HAYNES® 214™ joints ($d = 0.5$ mm) (a) L1 and (b) L2.

3.9 ± 0.4 MPa $m^{1/2}$ at 50 μm from the interface, while, for Al_2O_3/Cu–Ni–Cu/HAYNES® 214™ joints, K_{IC} only drops to about 4.5 ± 0.2 MPa $m^{1/2}$ at 50 μm from the interface. This decrease in apparent-toughness already was observed for many metal–ceramics systems[51–53] but not yet fully understood. It seems to be related to residual stresses and to diffusion of metallic specie, particularly along grain boundaries[51] (but note that the diffusion also leads to stresses in the crystal lattice and grain boundaries!). According to our previous diffusion studies by SIMS[53] (in particular for copper in alumina), diffusion from a thin metallic layer is observed and alumina toughness was lowered by the diffusion of metallic elements. This fall is about 2 MPa $m^{1/2}$ for the diffusion of copper, so relatively close to what we see here. The effect of diffusion is thus significant and can be superimposed on thermo-mechanical stresses due to the bonding.

Conversely, an increase in toughness is observed in both systems, from 100 μm from the interface up to 250 μm (Fig. 12a). These distances are greater than the penetration by diffusion along grain boundaries.[53] Other independent measurements show that the properties of alumina are strongly modified, from the metal–ceramic interface to over 250 μm, namely:

- In terms of dielectric properties,[54] from 0 to 50 μm, where the toughness is very low, the ability to trap electric charges, in alumina is high; on the other hand, in the area of toughening (100–250 μm), diffusion of electric charges is significant and local trapping is low.
- As noted above, the curves $\varepsilon_{\varphi\psi} = f(\sin^2 \psi)$ are abnormal in the toughening zone, which corresponds to a strong gradient of properties and, therefore the stress measurements contain errors.

Thus this toughening can be due to the stress field evolution, which may induce possibly a micro-cracking. In fact, both stresses and micro-cracking are favorable to diffusion of electric charges.

Fig. 12b shows the residual stresses estimation, in both joints, by using relation (5): near the interface, the residual stresses in Al_2O_3/Ni/HAYNES® 214™ joint are higher than for Al_2O_3/Cu–Ni–Cu/HAYNES® 214™, but the general trend observed for the two systems as function of the distance to the interface is similar. A strong variation of σ_{yy} is observed: i.e. stress decreases from $+318 \pm 34$ (near to the interface, ~20 μm) to -140 ± 35 (far from the interface, ~400 μm) for Al_2O_3/Ni/HAYNES® 214™ joint and from $+245 \pm 22$ MPa (near to the interface, ~20 μm) to -100 ± 12 MPa (far from the interface, ~400 μm) for Al_2O_3/Cu–Ni–Cu/HAYNES® 214™.

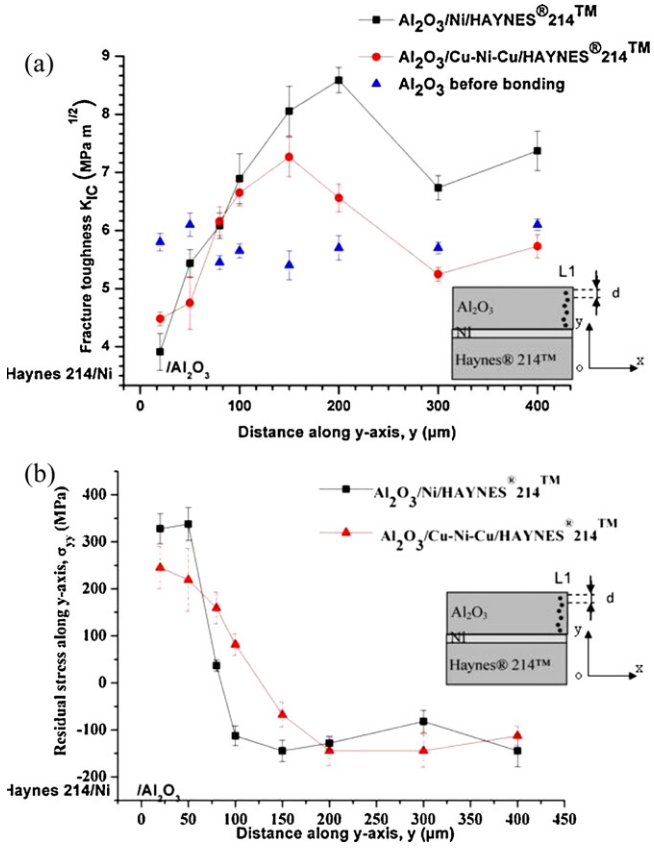

Fig. 12. Evolution of alumina fracture toughness and average residual stress with distance from interface for Al_2O_3/Ni/HAYNES® 214™ and Al_2O_3/Cu_2O–Cu/Ni/Cu/HAYNES® 214™ joints. (a) Fracture toughness and (b) residual stress. *d* is the distance between two Vickers indents.

3.2.3. Comparison VIF-XRD

Fig. 13 shows comparison of the results obtained for the residual stress distributions on the alumina ceramic near to the interface as given by two different methods; Vickers Indentation Fracture (VIF) method and X-ray diffraction method. In the case of Al_2O_3/Cu–Ni–Cu/HAYNES® 214™ system, both methods show qualitatively that residual stresses (σ_{yy}) were mainly

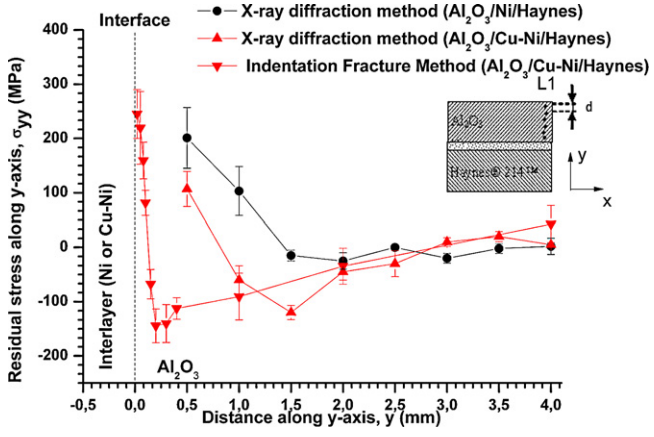

Fig. 13. Comparison of the results obtained for the residual stress distributions on the alumina ceramic near to the interface as given by two different methods; Vickers Indentation Fracture (VIF) method and X-ray diffraction through the L1.

tensile and the maximum was in the vicinity of the Cu–Ni/Al_2O_3 interface. After, pass from tension to compression (~1.5 mm from interface) and becomes almost constantly null far to the interface (>2.5 mm). In the case of Al_2O_3/Ni/HAYNES® 214™ system, the comparison is more difficult. Several reasons may explain these differences, namely:

- All measurements of stresses (or more accurately estimates) are indirect, for example, deformations are measured to estimate stresses, using assumptions more or less verified. Both techniques are no exception to this general remark.
- XRD can not measure stresses near the interface, since the first measurements are performed at 0.5 mm from the interface due to limited spatial resolution of the technique (~800 μm) and moreover, the measures are flawed below 1 mm, due to a complex stress field, as reported previously. The XRD estimate does not account for the strong evolution of the properties of ceramics in the vicinity of the interface, as demonstrated by both toughness and dielectric measurements. It is the same for finite element calculation.[1]
- Conversely, the estimated VIF stresses, from the toughness measurements, are very much dependent on them and therefore, have to be analyzed carefully. The VIF method, therefore, provides data in areas where the XRD measurements are ineffective: thus, the effect of the nickel diffusion in alumina on residual stresses cannot be identified.

Thus, these observations show the difficulty of measuring or calculating residual stresses in areas where the stress field is complex, with strong properties and stresses gradients, as is the case along the line L1, near the free edges of the assembly.

3.3. Mechanical testing

For Al_2O_3/Ni/HAYNES® 214™ system, after cooling from the bonding temperature, it is important to recall that, in some cases, the residual stresses typically cause cracking in the alumina ceramic[4] (Fig. 14). The perimeter crack initiates at some distance from the interface depending on the distribution and magnitude of residual stresses in each joint. On the other hand, in the case of Al_2O_3/Cu–Ni–Cu/HAYNES® 214™ joint, no cracks were observed after cooling.

3.3.1. Shear testing

The shear test specimens were prepared following the procedures described in Section 2.3. Results shown in Table 3 represent average shear strength data for joined samples for different interlayer thickness. For Al_2O_3/Ni/HAYNES® 214™ joints the shear strength ranges from 11 to 35 MPa and are modest compared to those of the Al_2O_3/Ni/Al_2O_3 joining.[1] The main difference between the mechanical behavior of both joints cited above are explained by the residual thermal stresses due to the CTE mismatch which magnitude depending on geometrical parameter shape which in certain case creates the critical defects such as perimeter crack or un-bonded zones at the interface similar to those shown in Fig. 14. The fractographic observations of the shear specimens confirmed that the crack is initiated close to

Table 3
Effect of Ni and Cu interlayers thickness on strength of both Al_2O_3/Cu_2O–Cu/Ni/Cu/HAYNES® 214™ and Al_2O_3/Ni/HAYNES® 214™ joints under shear test loading.

Joint[a]	Shear strength (MPa)	Ni thickness (mm)	Cu thickness (mm)
Al_2O_3/Ni/HAYNES® 214™	11 ± 3	0.1	–
	25 ± 2	0.2	–
	28 ± 2	0.3	–
	35 ± 4	0.5	–
Al_2O_3/Cu_2O–Cu/Ni/Cu/HAYNES® 214™	82 ± 6	0.1	0.1
	68 ± 5	0.2	0.1

[a]For all cases, $R' = Ec/Ea = 1$, ratio between the thickness of the ceramics and the thickness of the alloy (Ea = 5 mm).

the free edge of the sample, on defects located in the Ni/Al_2O_3 interface and then changes its direction, and propagates into the ceramics bulk, near the interface, with a "crack-interface" angle, equal to about 40° corresponding approximately to the direction of the maximal tensile stress determined by FEA.[1,4]

Al_2O_3/Ni/HAYNES® 214™ samples show poor mechanical strength when compared with Al_2O_3/Cu_2O–Cu–Ni–Cu/HAYNES® 214™ (Table 3). The average strength of this later was significantly higher than that of joints with a single Ni interlayer. As a result of observation of the fracture surface, the crack occurred in the ceramic along path that was extremely close to the interface (∼10 μm).

These results are consistent with our measurements of residual stresses since the stress components most significant in fracture of ceramic–metal joints are the tensile and shear stresses at the free edge.

3.3.2. Four-point 'delamination' bending test

Strength measurements of ceramic–metal joints are important to provide information on the mechanical integrity of the joints. In this context, some bend tests (delamination) at ambient temperature were conducted on the Al_2O_3/Ni/HAYNES® 214™ and Al_2O_3/Cu_2O–Cu/Ni/Cu/HAYNES® 214™ joints. During fracture tests, the applied displacement and the corresponding load values were recorded. Fig. 15 shows a typical relationship between the load P and displacement u in the case of Al_2O_3/Cu_2O–Cu/Ni/Cu/HAYNES® 214™ joints. Several steps are indicated and described as follows:

(a) the load increased proportionally to displacement; in this stage, no crack propagation occurs and the crack opening at the centre is very small;
(b) the interfacial delamination occurred on one side of the sample and a load plateau is observed. The left side of the crack propagates while the right side of the crack did not propagate. This situation of asymmetrical crack growth was clearly visible on the specimen;
(c) the load again increases proportional to the displacement. Compared to the region (a), the compliance of the sample increased, due to the previous crack growth event;
(d) a second load plateau occurred, which corresponds to a crack growth along the right side. The opening of both cracks is similar. Segmentation cracks and micro-cracks appeared along the Cu_2O/Al_2O_3 interface and on the top of alumina surface. Thus, the alumina (Al_2O_3) still adhere to the substrate (HAYNES® 214™);
(e) finally, the sample compliance has increased further due to the additional crack growth along the right side.

For Al_2O_3/Ni/HAYNES® 214™ joints the same steps are observed but in the zone (*d*), in spite of its separation from Ni foil, the alumina are still compact (i.e. no micro-cracks appeared on Ni/Al_2O_3 interface or on alumina surface

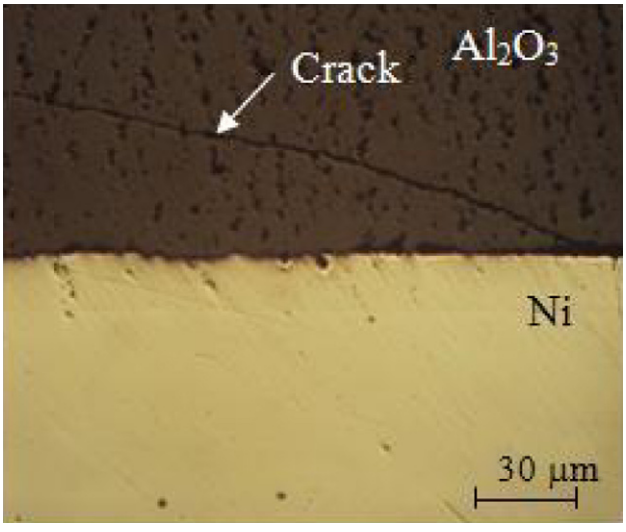

Fig. 14. Crack propagation in alumina ceramic in the Al_2O_3/Ni/HAYNES® 214™ system alter joining process.

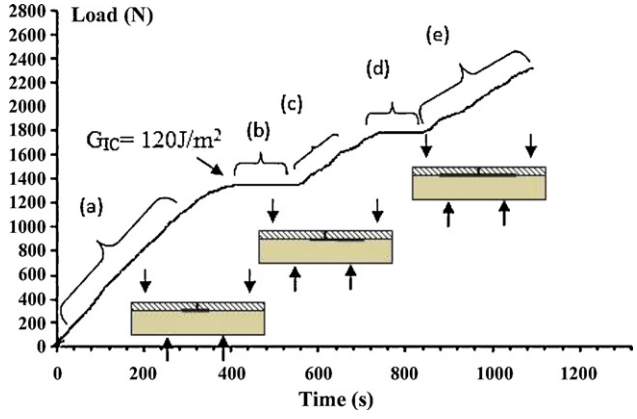

Fig. 15. Typical load–time curve in the four-point bending test for the Al_2O_3/Cu_2O–Cu/Ni/Cu/HAYNES® 214™ joints.

Table 4
Critical interfacial fracture energy for both Al_2O_3/Cu_2O–Cu/Ni/Cu/HAYNES® 214™ and Al_2O_3/Ni/HAYNES® 214™ joints under mixed-mode loading (delamination bending test).

Joint	Al_2O_3 thickness (mm)	Experimental conditions[a]	G_{IC} (J/m^2)
Al_2O_3/Ni/HAYNES® 214™	0.381	$R' = 0.08$	0
	0.635	$R' = 0.13$	1.5 ± 0.5
Al_2O_3/Cu–Ni–Cu/HAYNES® 214™	0.381	$R' = 0.08$	122 ± 8
	0.635	$R' = 0.13$	89 ± 12

[a] R' = Ec/Ea, ratio between the thickness of the ceramics and the thickness of the alloy (Ea = 5 mm). Ni interlayer thickness is 0.2 mm and Cu interlayer thickness is 0.1 mm.

top). All the Al_2O_3/Cu_2O–Cu/Ni/Cu/HAYNES® 214™ and Al_2O_3/Ni/HAYNES® 214™ specimens broke with a non-linear curve "load–deflexion", at the ceramic–metal interface. The presence of this effect could be due to the thickness of the metal (metal foils + HAYNES® 214™ alloy ∼5.3 mm).

For Cu/Ni/Cu interlayer, the ceramic side of the fracture surface at the interface between Al_2O_3 and Ni shows that Al_2O_3 contains some small particles (about 2–8 μm) of Cu_2O. On the metal side, some Al_2O_3 grains are attached to copper.

In Table 4, the mean values and the standard deviations of fracture energy are reported. Sample Al_2O_3/Ni/HAYNES® 214™ shows poor mechanical strength when compared with Al_2O_3/Cu_2O–Cu/Ni/Cu/HAYNES® 214™. This high value of fracture strength and the corresponding energy (122 J/m^2) obtained for this system induce good mechanical adhesion correlated not only with the presence, at the interface, of a favorable reaction product ($CuAlO_2$), but also with lower residual stresses. By contrast, high residual stresses and growth of the spinel nickel aluminate in Al_2O_3/Ni/HAYNES® 214™ joint were previously found to be damaging to the strength of the interface.[55]

3.3.3. *Effect of Ni and Cu/Ni/Cu interlayer thicknesses on mechanical strength*

It is well known that joint strength depends on the thickness of the joining layer[4] which affects the magnitude of the residual stress (due to the properties of the third material). In the case of Al_2O_3/Ni/HAYNES® 214™ system, the shear strength increases with increasing Ni interlayer thickness (Table 3). In every case, the fracture propagates into the ceramic (cohesive fracture). In contrast, in the case of Al_2O_3/Cu_2O–Cu/Ni/Cu/HAYNES® 214™ joints, the decrease in thickness of Ni interlayer, for constant Cu interlayer, leads to an increase in the shear strength and the fracture occurred in Al_2O_3/Cu–Cu_2O interface (adhesive fracture) (Table 3).

Thus, interfacial failure of both bonds is clearly dependent on metal layer thickness. The variation within the general range of strength obtained at each thickness reflects residual stress effect.[4] The trend to low strength with thin metal layer derives from the increasing influence of the corner stress concentration.

The interfacial fracture energies measured for both joints are summarized in Table 4. As shown previously,[4] residual stresses and both fracture energies depend on the thickness of the ceramics or, more accurately, on the ratio R' between the thickness of the ceramics and the thickness of the alloy "Ec/Ea": Ec/Ea < 1 is recommended.[4]

4. Conclusions

The residual stresses, in dissimilar metal/ceramic bonds, has been evaluated by measuring residual stresses using of X-ray diffraction (XRD) and Vickers Indentation Fracture (VIF). In particular, VIF confirms that changes in the nature of alumina in the immediate vicinity of the interface occur during bonding processes, which can lead to technological difficulties too often disregarded, i.e. mechanical properties, but dielectric properties too. This is confirmed in another paper,[54] on the same systems.

The whole map of the residual stress field in the ceramic is obtained by measuring along scanning lines perpendicular to the metal–ceramics interface. Maximum tension in ceramics occurs near the free edge of the interface, where the stresses are singular. It is this tensile stress developed in ceramics that is the most important factor inducing the joint failure. This is believed to be the main cause of the modest shear and bend strength values obtained for Al_2O_3/Ni/HAYNES® 214™ system.

To overcome this problem, ideas concerning the best configuration of such interlayers differ and include use of multi-component systems combining graded expansion and/or ductility e.g. Cu–Ni, Cu–Mo.[29] The use of multiple interlayers such as Cu–Ni–Cu can create even greater reduction in strain energy by redistributing the stress and plastic strain in a ductile interlayer Cu next to the ceramic. Our experiments show the beneficial of Cu–Ni–Cu multilayers to reduce residual stresses and enhance mechanical behavior of the joint.

In addition, our experiences on joining alumina to HAYNES® 214™ via nickel–copper inserts, can show that it is possible to reduce both temperature and pressure classically used for solid state bonding. For the Al_2O_3/Cu_2O–Cu/Ni/Cu/HAYNES® 214™ systems, the processing temperature reductions are on the order of several hundred degrees. The choice of copper presents the advantage, using the DCB technique, to make the bonding under a very weak applied load during the process (<1 MPa unlike 16 MPa for solid state bonding), thanks to the formation of a transitory liquid film.

Moreover, the Cu–Ni system exhibits complete mutual solid solution at elevated temperature. Consequently a post-annealing at 1150 °C should lead to the formation of a uniform Ni-rich Cu–Ni solid solution in the interlayer region. If the Cu concentration in the Ni is below 50 wt. %, this interlayer has a melting temperature of approximately 1200 °C, producing a high-temperature ductile interlayer. Thus, this process makes

it possible to obtain metal–ceramics joints ready to resist at high temperatures.

References

1. Hattali ML, Valette S, Ropital S, Mesrati N, Tréheux D. Calculation and experimental determinations of the residual stress distribution in alumina/Ni/alumina and alumina/Ni/nickel alloy systems. *J Mater Sci* 2010;**45**(15):4133–40.
2. Hattali ML, Valette S, Ropital S, Mesrati N, Tréheux D. Study of SiC–nickel alloy bonding for high temperature applications. *J Eur Ceram Soc* 2009;**29**:813–9.
3. Martinelli AE, Drew RAL. Microstructural development during diffusion bonding of α-silicon carbide to molybdenum. *J Mater Sci Eng A* 1995;**191**(1):239–47.
4. Hattali ML, Valette S, Ropital S, Mesrati N, Tréheux D. Effect of thermal residual stresses on the strength for both alumina/Ni/alumina and alumina/Ni/nickel alloy bimaterials. *J Mater Sci* 2009;**44**: 3198–210.
5. Larson DS, Adams JW, Johnson LR, Teotia APS, Hill LG. *Ceramic materials for advanced heat engines*. Park Ridge, NJ: Noyes; 1985.
6. Shalz ML, Dalgleich BJ, Tomsia AP, Glaeser AM. Ceramic joining. I. Partial transient liquid-phase bonding of alumina via Cu/Pt interlayers. *J Mater Sci* 1993;**28**(6):1673–84.
7. Shalz ML, Dalgleich BJ, Tomsia AP, Glaeser AM. New approaches to joining ceramics for high-temperature applications. *Ceram Trans* 1993;**35**:301–22.
8. Shalz ML, Dalgleich BJ, Tomsia AP, Cannon RM, Glaeser AM. Ceramic joining II partial transient liquid-phase bonding of alumina via Cu/Ni/Cu multilayer interlayers. *J Mater Sci* 1994;**29**(14):3200–8.
9. Tomsia AP. Ceramic/metal joining for structures and materials. *J Phys IV* 1993;**3**(C7):1317–26.
10. Tomsia AP, Leohman RE. Reactions and microstructure at selected ceramic/metal interfaces. *Mater Manuf Process* 1994;**9**(3): 547–61.
11. Nicholas MG. *Joining of ceramics*. London: Chapman & Hall; 1990.
12. Klomp JT. Interfacial reactions between metals and oxides during sealing. *Am Ceram Bull* 1980;**59**(8):794.
13. Nicholas MG. In: Peteves SD, editor. *Joining Structure Ceramics in Designing Interfaces for Technological Applications*. London, UK: Elsevier; 1989.
14. Fernie JA, Threadgill PL, Watson MN. Progress in joining of advanced materials. *J Weld Met Fabricat* 1991;**1**:179–84.
15. Maloletov MP. Theoretical fundamentals and technology of electron beam welding ceramics to metals. *J Weld Int* 1995;**64**(3):237–9.
16. Matsuoka S. Ultrasonic welding of ceramics/metals using inserts. *J Mater Process Technol* 1998;**75**(2):259–65.
17. Hokamoto K, Fujita M, Shimokawa H. A new method for explosive welding of AI/ZrO_z joint using regulated underwater shock wave. *J Mater Process Technol* 1999;**85**(1):175–9.
18. Nicholas MG. Active metal brazing. *J Ceram Trans* 1986;**85**(1):144–6.
19. Nicholas MG, Crispin RM. Diffusion bonding stainless steel to alumina using aluminium interlayers. *J Mater Sci* 1982;**17**(11):3347–60.
20. Zhang JX, Chandel RS, Chen YZ, Seow HP. Effect of residual stress on the strength of an alumina–steel joint by partial transient liquid phase (PTLP) brazing. *J Mater Process Technol* 2002;**122**:220–5.
21. Honglong N, Jusheng M, Fuxiang H, Yonggang W, Qianqian L, Xiaoyan L. Preoxidation of the Cu layer in direct bonding technology. *Appl Surf Sci* 2003;**211**:250–8.
22. Zhang Y, Feng D, He ZY, Chen XC. Progress in joining ceramics to metals. *J Iron Steel Res Int* 2006;**13**(2):01–5.
23. Dalgleish BJ, Trumble KP, Evans AG. The strength and fracture of alumina bonded with aluminum alloys. *Acta Metall* 1989;**37**(7):1923–31.
24. Zhang JX, Chandel YZ, Seow HP. Effect of residual stress on the strength of an alumina–steel joint by partial transient liquid phase (PTLP) brazing. *J Mater Process Technol* 2002;**122**:220–5.
25. Lourdin P, Juvé D, Tréheux D. Nickel-alumina bonds: mechanical properties related to interfacial chemistry. *J Eur Ceram Soc* 1996;**16**(7):745–52.
26. Drory M, Evans A. Experimental observations of substrate fracture caused by residually stressed films. *J Am Ceram Soc* 1990;**73**(3):634–8.
27. Lee SB, Kim JH. Finite elements analysis and X-ray measurement of the residual stress of ceramic/metal joints. *J Mater Process Technol* 1997;**67**:167.
28. Tréheux D, Fayeulle S, Guipont V, Jacquemin JP. In: Bellosi A, editor. *Interfacial Science in Ceramic Joining*. Kluver Academic Publishers; 1989. pp. 311–318.
29. Dalgleish BJ, Lu MC, Evans AG. The strength of ceramics bonded with metals. *Acta Metall* 1988;**36**(8):2029–35.
30. Nemoto Y, Ueda K, Satou M, Hasegawa A, Abe K. Analysis and measurements of residual stress distribution of vanadium/ceramics joints for fusion reactor applications. *J Nucl Mater* 1998;**258-163**:1517–22.
31. Colin C. Les assemblages métal-céramique. *Thesis Ecole des mines de Paris*; 1991.
32. Burgess JF, Neugebauer CA, Flanagan G. Direct bonding of metals to ceramics by the gas–metal eutectic method. *J Electrochem Soc* 1975;**122**(5):688–90.
33. Sun YS, Driscoll JC. A new hybrid power technique utilizing a direct copper to ceramic bond. *IEEE Trans Electron Devices* 1976;**23**(8):961–7.
34. Jürgen SH.*Proceedings of 3rd electronics packaging technology conference*. 2000. p. 315.
35. Catellani S, Crebier JC, Schaeffer C, Marsala T. Thermal and electrical aging of DBC substrates. In: *Proc. IEEE PESC'01*. 2001.
36. Hong H, Renli F, Deliu W, Xiufeng S, Min J. A new method for preparation of direct bonding copper substrate on Al_2O_3. *Mater Lett* 2007;**61**(19–20):4131–3.
37. Agathopoulos S. Interfaces in bioceramics: surface energetics and interfacial interactions. *Key Eng Mater* 2002;**224-226**:417–24.
38. Agathopoulos S, Tulyaganov DU, Ferreira JMF. Stages of reactive wetting. *Key Eng Mater* 2005;**280-283**:1801–4.
39. Kang JC, Yoon J, Min K. A highly linear and efficient differential CMOS power amplifier with harmonic control. *IEEE J Solid-State Circuits* 2006;**41**(6):1314.
40. Agathopoulos S, Pina S, Correia RN. A review of recent investigations on zirconia joining for biomedical applications. *Ceram Trans* 2003;**138**: 135–45.
41. Beraud C, Courbiere M, Esnouf C, Juvé D, Tréheux D. Study of copper–alumina bonding. *J Mater Sci* 1989;**24**:4545–54.
42. Tréheux D, Lourdin P, Mbongo B, Juvé D. Metal–ceramic solid state bonding: mechanisms and mechanics. *Scripta Metall Mater* 1994;**31**(8): 1055–60.
43. Kara-Slimane A, Mbongo B, Tréheux D. Adhesion and reactivity in the copper–alumina system. *J Adhes Sci Technol* 1999;**13**:35–48.
44. Charalambides PG, Lund J, Evans AG, Mcmeeking RM. A test specimen for determining the fracture resistance of bimaterial interfaces. *J Appl Mech* 1989;**56**:77–82.
45. Laribi M, Vannes AB, Mesrati N, Tréheux D. Adhesion and residual stresses determination of thermally sprayed molybdenum on steel. *J Surf Coat Technol* 2003;**166**(2):206.
46. Liang KM, Orange G, Fantozzi G. Determination of Kscc by indentation in ceramics. *J Mater Sci* 1990;**25**(1):207–14.
47. Lawn BR, Fuller ERJR. Measurement of thin-layer surface stresses by indentation fracture. *J Mater Sci* 1989;**19**:4061–7.
48. Esposito L, Bellosi A, Guicciardi S, De portu G. Solid state bonding of Al_2O_3 with Cu, Ni and Fe: characteristics and properties. *J Mater Sci* 1998;**33**(7):1827–36.
49. Kubashewski O, Alock B. *Metallurgical thermochemestry*. 5th ed. Elmsford, NY: Pergamon Press; 1979.
50. Reimanis IE, Trumble KP, Rogers KA, Dalgleish BJ. Influence of Cu_2O and $CuAlO_2$ interphases on crack propagation at Cu/α-Al_2O_3 interfaces. *J Am Ceram Soc* 1997;**80**(2):424–32.
51. Serier B, Tréheux D. Silver-alumina solid state bonding: influence of the work hardening of the metal. *Acta Metall Mater* 1993;**41**(2):369–74.
52. Juvé D, Lourdin P, Mbongo B, Boukheit N, Tréheux D. Damages and cracks in ceramic/metal interfaces. *J Phys IV* 1993;**3**:1057–60.

53. Moya-Gontier E, Moya F, Sami A, Boukheit N, Juvé D, Tréheux D. Relationship between the nature of dopants and charging or mechanical properties of ceramics. In: *Conference of electrical insulation and dielectric phenomena (CEIDP), IEEE annual report*. 1995. p. 664–7.
54. Hattali ML, Mesrati N, Tréheux D. Electric charge trapping, residual stresses and properties of ceramics after metal–ceramics bonding. *J Eur Ceram Soc* 2012;**32**(4):717–25.
55. Naidich Yu. Wettability of solids by liquid metals. *Prog Surf Membrane Sci* 1981;**14**:353.